Heliyon 6 (2020) e03202

Contents lists available at ScienceDirect

Heliyon

journal homepage: www.cell.com/heliyon

Research article

Low-cost supercapacitor based on multi-walled carbon nanotubes and activated carbon derived from *Moringa Oleifera* fruit shells

Shirley Palisoc [a,b], Joshua Marco Dungo [a], Michelle Natividad [a,b,*]

[a] Condensed Matter Physics Laboratory, De La Salle University, Manila, 922, Philippines
[b] Condensed Matter Research Unit, CENSER, De La Salle University, 2401 Taft Avenue, Manila, 922, Philippines

ARTICLE INFO

Keywords:
Materials science
Energy sustainability
Materials application
Materials characterization
Nanomaterials
Supercapacitor
Multi-walled carbon nanotubes
Activated carbon
Moringa oleifera fruit shells

ABSTRACT

An electric double-layer capacitor (EDLC) was fabricated using multi-walled carbon nanotubes (MWCNT) and activated carbon (AC) derived from *Moringa Oleifera* fruit shells as electrode material. The carbonization temperature and the weight ratio of the fruit shells to the activating agent were varied to determine the best condition in the fabrication of the electrodes. Activation of the carbonized fruit shells by $ZnCl_2$ resulted in the formation of pores as verified by the scanning electron micrographs. Energy dispersive X-ray analyses show that the washing of the carbonized sample resulted in the removal of zinc and chlorine residues. The supercapacitor electrodes were fabricated by adding polyvinylidene fluoride and N-methylpyrrolidone to the MWCNT-AC mixture to form a slurry and was cast onto a nickel foam. The capacitance of the fabricated electrodes was determined using a potentiostat. The activated carbon with a carbonization temperature of 800 °C and a 1:2 weight ratio between the fruit shells and $ZnCl_2$ was observed to have the highest capacitance of 130 F g^{-1} and was duplicated to fabricate the supercapacitor electrodes. A glass microfiber filter was soaked in 3 M KOH and placed in between the two electrodes. The specific capacitance of the EDLC was found to be 122 F g^{-1} at a current density of 0.5 A g^{-1}, average energy density of 17 W h kg^{-1}, average power density of 1.5 kW kg^{-1} and an equivalent series resistance of 1.6 Ω. After 100 scans with a scan rate of 0.1 V s^{-1}, the percent decrease in capacitance was calculated to be 2.65 % of its original capacitance.

1. Introduction

Electricity is the most sought-out form of energy, the need for which is very ubiquitous in almost everything that people use. Powering devices, motors, and other equipment in today's standards mostly require electricity. Currently, fossil fuels are the world's major source of electricity. However, burning fossil fuels emits harmful products which are hazardous to human health and the environment. In order to reduce the world's dependence on fossil fuels and to deal with the imminent depletion of these nonrenewable resources, other energy sources and storage technologies are being developed [1, 2, 3].

Stored energy has always been an inherent necessity for the advancement of technology. Gaining and delivering energy instantaneously is widely sought after, particularly in the automotive industry. Interestingly, the existing technology to address the aforementioned need is the supercapacitor. Supercapacitors are capacitors with high capacitance and have high energy density. What sets supercapacitors apart from batteries is that while batteries have the ability to store energy for longer usage, supercapacitors can be charged and discharged quickly, hence, they have a very high power density [4]. Given their differences in function, making one totally distinct from the other can be an unnecessary endeavor. For application purposes, sometimes both are even used together [5].

The two types of supercapacitors are the pseudocapacitors and the electrostatic double-layer capacitors (EDLC). Pseudocapacitors have a chemical reaction at the electrode and store charge electrochemically while EDLCs use carbon electrodes with a high double layer capacitance and store charge electrostatically [6, 7, 8]. This type of capacitor contains no conventional dielectrics. Alternatively, an electrolyte is placed between the two electrodes [9, 10, 11, 12]. The charge and discharge of an EDLC are mechanically contributed by the absorption and desorption to the electrical double layer. Given that both types of capacitors are very costly to make, thus making the need for the less expensive ones indeed an urgency. At present, activated carbon (AC) derived from biomass materials such as corncobs [13], enteromorpha [14], hemp [15], infested ash trees [16], loofah sponges [17], melons [18], olive pits [19],

* Corresponding author.
E-mail address: michelle.natividad@dlsu.edu.ph (M. Natividad).

https://doi.org/10.1016/j.heliyon.2020.e03202
Received 28 September 2019; Received in revised form 8 December 2019; Accepted 8 January 2020

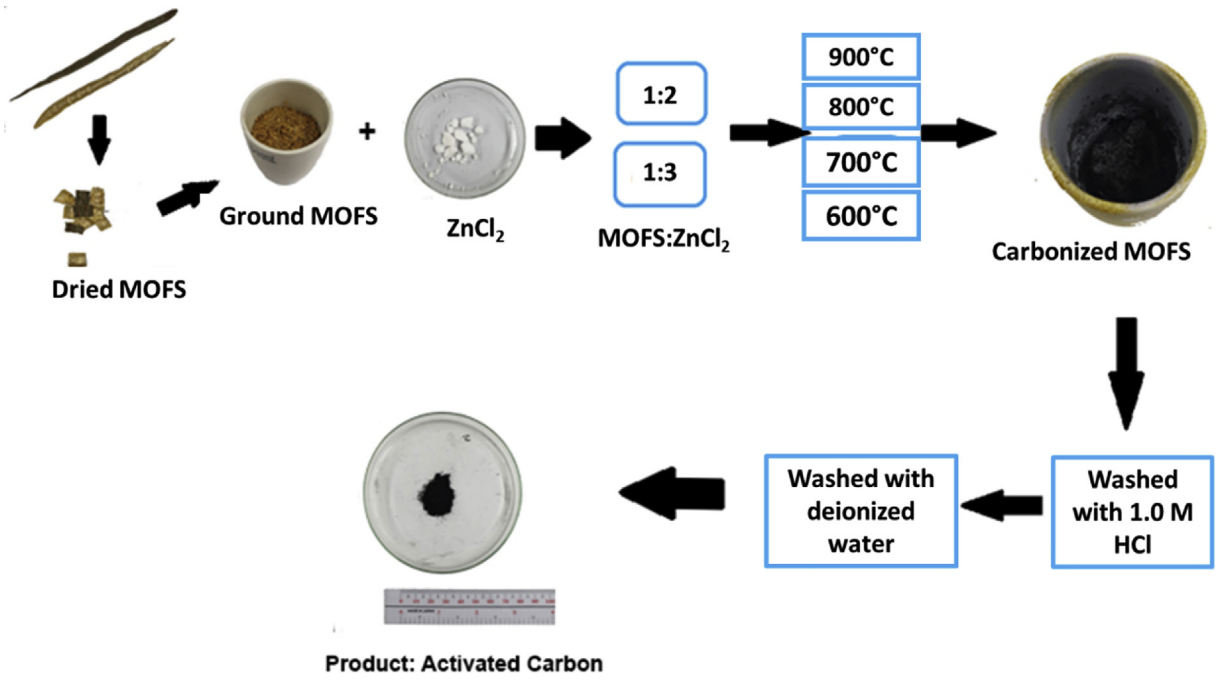

Figure 1. Schematic diagram of the activation process of Moringa Oleifera fruit shells.

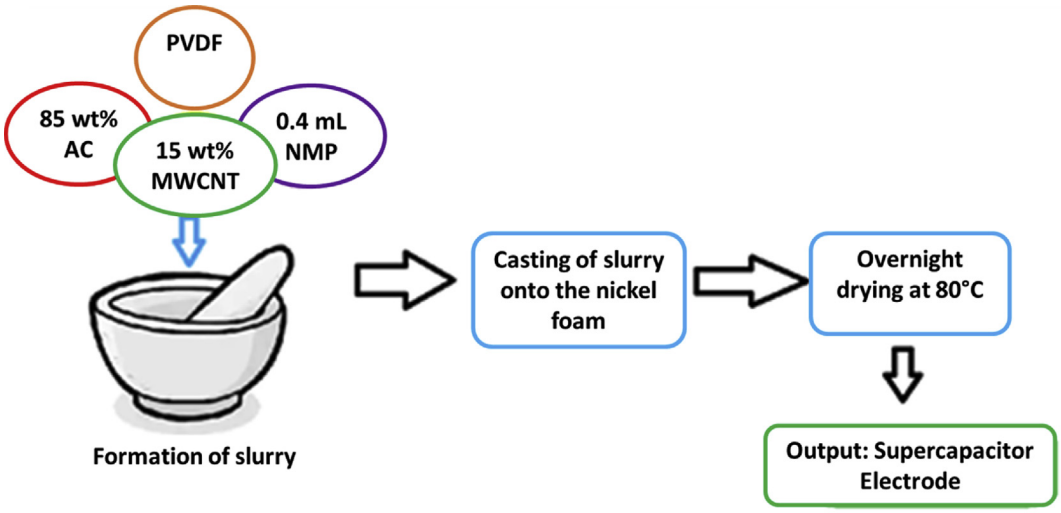

Figure 2. Schematic diagram of supercapacitor electrode fabrication.

pinecones [20], peanut shell [21], rice husk [22], starch [23], shiitake mushrooms [24], tobacco waste [25], and willow catkins [26], have been employed as carbon precursors for fabricating electrode materials for supercapacitors due to their abundance, renewability, low-cost and environment friendly properties. In previous studies [27, 28], addition of multi-walled carbon nanotubes (MWCNT) to commercially available activated carbon increased the energy density and specific capacitance of supercapacitor cells. The increase is attributed to the large surface area of the AC and the good conducting property of the MWCNT network.

Table 1. Identification of AC samples based on their variations.

Sample	A	B	C	D	E	F	G
Carbonization Temperature	600 °C	600 °C	700 °C	700 °C	800 °C	800 °C	900 °C
MOFS to $ZnCl_2$ ratio	1:3	1:2	1:3	1:2	1:3	1:2	1:2

Moringa Oleifera, also known as the drumstick tree, is a fast-growing deciduous tree. It is native to India but has been planted in other countries such as the Philippines, Africa, and South America [29]. It belongs to the family of *Moringaceae* which is abundant in nature and produces highly nutritious fruits [30]. The shells or pods of the *Moringa Oleifera* fruits contain cellulose, hemicellulose, and lignin which are the essential components of precursors for the production of porous activated carbon that are well suited for electrochemical and energy storage applications [8].

This paper reports a facile method of preparing AC/MWCNT based electrodes for EDLC supercapacitors. The activated carbon was derived from *Moringa Oleifera* fruit shells (MOFS) which makes the supercapacitor not only cost-effective but environment-friendly as well. Characterization of the precursors and components of the supercapacitors was performed using scanning electron microscopy, energy dispersive X-ray spectroscopy, cyclic voltammetry, chronopotentiometry, and electrochemical impedance spectroscopy.

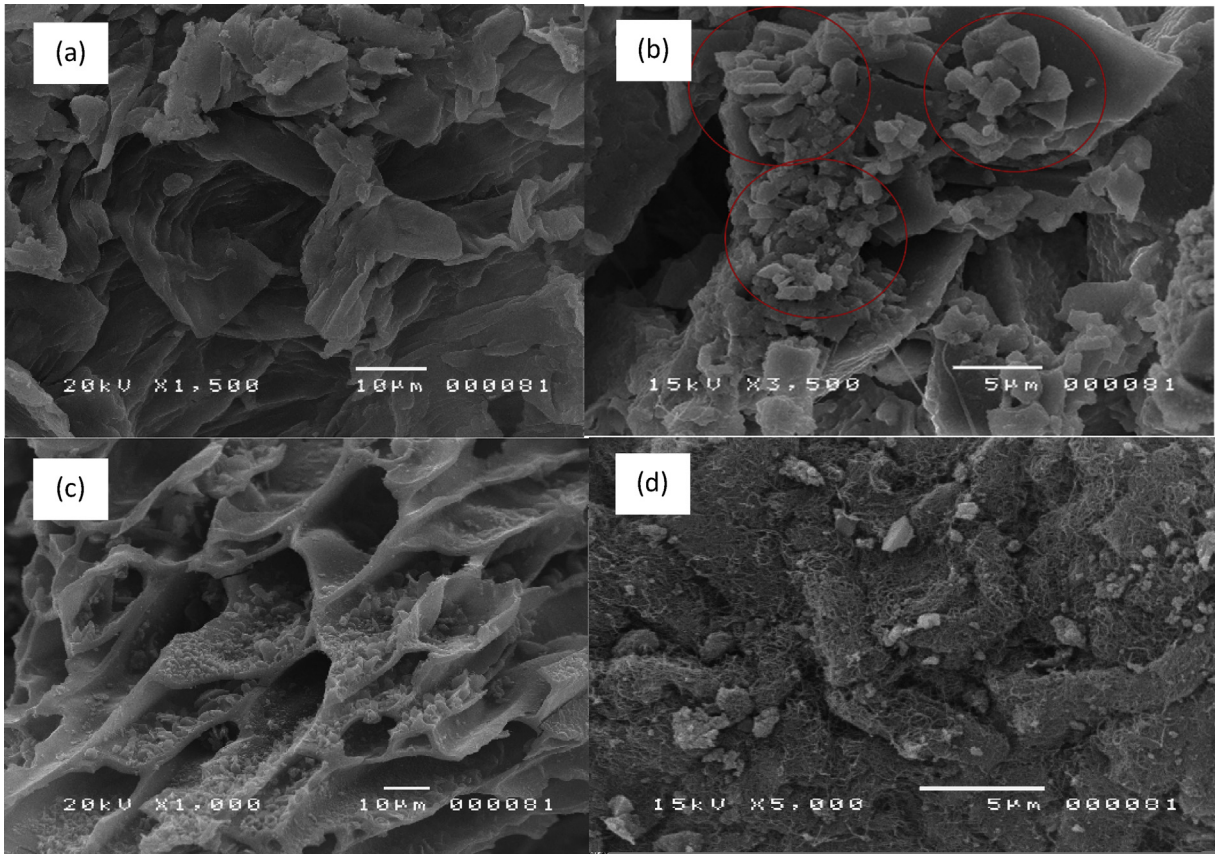

Figure 3. SEM images of (a) dried MOFS, (b) activated MOFS with $ZnCl_2$ residues (encircled in red), (c) activated MOFS with pore formation, and (d) AC/MWCNT.

2. Methodology

2.1. Reagents and solutions

The *Moringa Oleifera* fruit shells were sourced from a farm in Laguna, Philippines. Zinc chloride ($ZnCl_2$), potassium hydroxide (KOH), multi-walled carbon nanotubes (MWCNT), N-methylpyrrolidone (NMP), hydrochloric acid (HCl), and polyvinylidene fluoride (PVDF) were purchased from Sigma Aldrich (Singapore). The reagents were analytical grade and were used without further purification.

2.2. Preparation of activated carbon

The MOFS were sun-dried for a day. The dried fruit shells were cut into small pieces and weighed initially using a BOSCH SAE200 electronic balance. The weighed fruit shells were placed in a ceramic crucible and were dried in a furnace at 150 °C for 4 h. The oven-dried fruit shells were ground and a chemical activation agent, $ZnCl_2$, was added to the ground fruit shells. The MOFS to $ZnCl_2$ weight ratio was varied at1:2 and 1:3. The mixtures were divided into four and were subjected to different carbonization temperatures (600 °C, 700 °C, 800 °C, and 900 °C) for 5 h at a rate of 10 °C/min in a nitrogen atmosphere and then cooled to room temperature. The typical carbonization temperature range, 600 °C–900 °C, is where moisture, volatiles, and most of the non-carbon hetero-elements in biomass (oxygen, hydrogen, nitrogen, and sulfur) are removed resulting to a much higher carbon content [31]. The carbonized MOFS were then washed five times with 1.0 M HCl through a filter membrane to remove the $ZnCl_2$ impurities. It was then further washed with deionized water through a filter membrane five times to remove the HCl residue as shown in the schematic diagram in Figure 1.

2.3. Fabrication of electrodes

The electrodes were fabricated by mixing the generated AC (85 wt%) and MWCNT (15 wt%) with 0.4 mL of NMP and PVDF to form a homogenous slurry. The slurry was cast onto a nickel foam with a dimension of 1 cm × 1 cm and dried in a vacuum oven overnight at 80 °C Figure 2 shows a schematic diagram of the fabrication process.

2.4. Fabrication of the EDLC

A glass microfiber separator was soaked in a 3 M KOH electrolyte for 1 h. The fabricated electrodes were carefully placed on each side of the separator. Electrical tape was used to hold the electrodes and separator in place.

2.5. Electrochemical characterization

The electrochemical properties of the AC/MWCNT electrodes were assessed using cyclic voltammetry (CV), chronopotentiometry, and electrochemical impedance spectroscopy (EIS) on a PalmSens4 potentiostat. For the three-electrode system, the fabricated AC/MWCNT electrode served as the working electrode, an Ag/AgCl electrode as the reference electrode and a platinum wire as the counter electrode. For the two-electrode system, the fabricated EDLC was used. The electrolyte solution was composed of 1.0 M KOH. The CV scans for the three-electrode system were done in the potential range of -0.7 V–0.3 V, current density of 1 A g^{-1} and scan rate of 0.05 V/s for 3 cycles. For the two-electrode system, the CV curves were obtained at scan rates of 0.07, 0.1, 0.2, 0.3, and 0.5 V/s over the potential window of -0.8 to 0.4 V. The galvanostatic charge-discharge (GCD) curve was obtained over a potential range of -0.1 V–0.2 V and current density of 0.5 A g^{-1}. The EIS

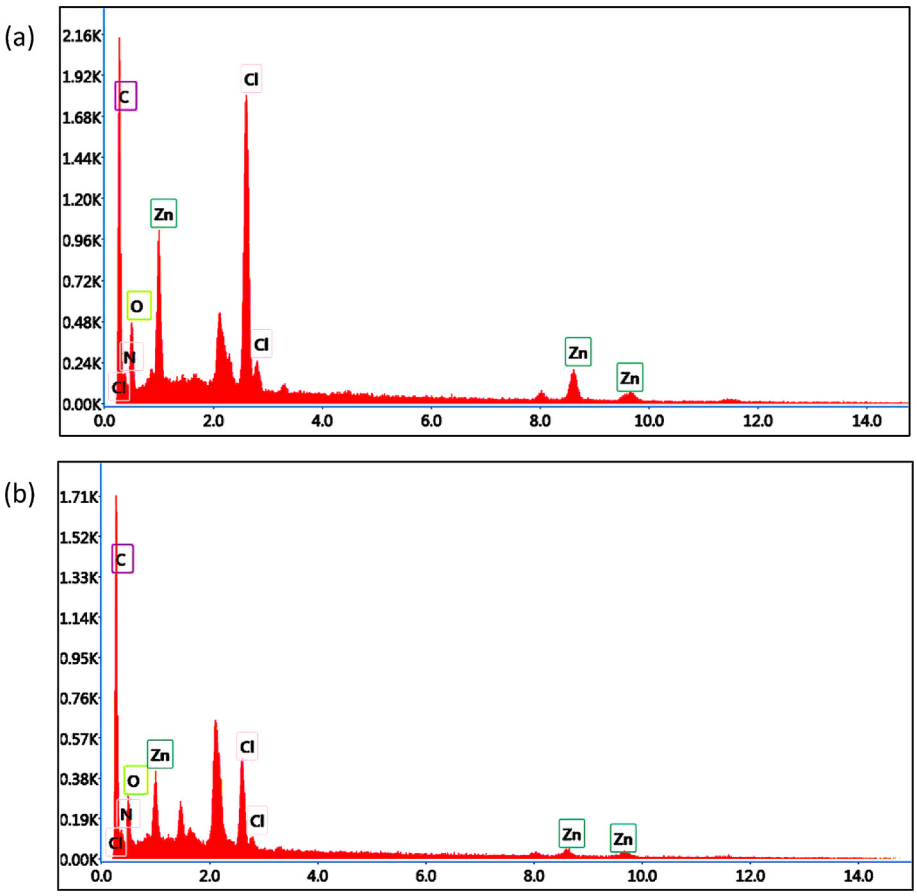

Figure 4. EDX results of the activated carbon (a) before and (b) after washing with HCl and deionized water.

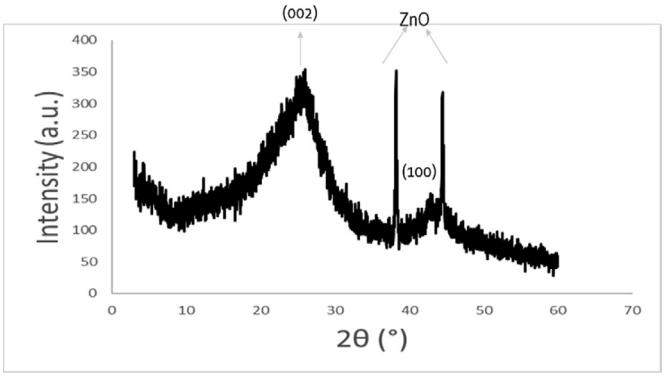

Figure 5. XRD spectrum of the AC/MWCNT sample.

measurements were carried out between the frequency range of 1 MHz and 100 Hz.

2.6. Physical characterization

A JSM-5310 JEOL scanning electron microscope coupled with energy dispersive X-ray spectroscopy was used to investigate the morphology and the elemental composition of the synthesized activated carbon. A BTX-285 x-ray powder diffractometer was used for the crystal structure analysis. The diffractometer consists of an X-ray tube, a sample holder, and an X-ray detector. The X-ray beam was collimated at an angle θ and the X-ray detector collect the diffracted X-rays at an angle of 2θ. A Fourier transform-infrared spectrometer was utilized for the identification of the chemical components of the samples.

3. Results and discussion

3.1. Determination of the best electrode

Seven different variations of activated carbon were produced to achieve the objective of determining the ideal amounts of MOFS and activating agent for optimum supercapacitor performance. The parameters that were varied are the carbonization temperature (600 °C, 700 °C, 800 °C, and 900 °C) and the weight ratio between MOFS and $ZnCl_2$ (1:3 and 1:2). Table 1 shows the identification of the AC samples based on their variations.

3.2. Physical characterization

The surface morphology of the MOFS prior to and after the activation process was studied using scanning electron microscopy. Figure 3a shows the SEM image of the dried MOFS. The surface is relatively rough with minimal signs of pore formations. The SEM image of the activated MOFS is shown in Figure 3b. It can be observed from the micrograph that residues of $ZnCl_2$ (encircled in red) are present on the surface of the activated MOFS. The disappearance of these $ZnCl_2$ residues which led to the formation of pores [32] is shown in Figure 3c. A more porous surface compared with the activated carbon without MWCNT is shown in Figure 3d. The MWCNT structures are visible, as evidenced by the string-like structures on the surface.

The elemental composition of the AC/MWCNT sample was analyzed using EDX. Figure 4a shows the elements that are present in the carbonized sample before it was washed with HCl and deionized water. The high percentage of carbon implies that most of the volatiles and non-carbon content of the MOFS were removed during the activation process which led to a much higher carbon content [31]. The high

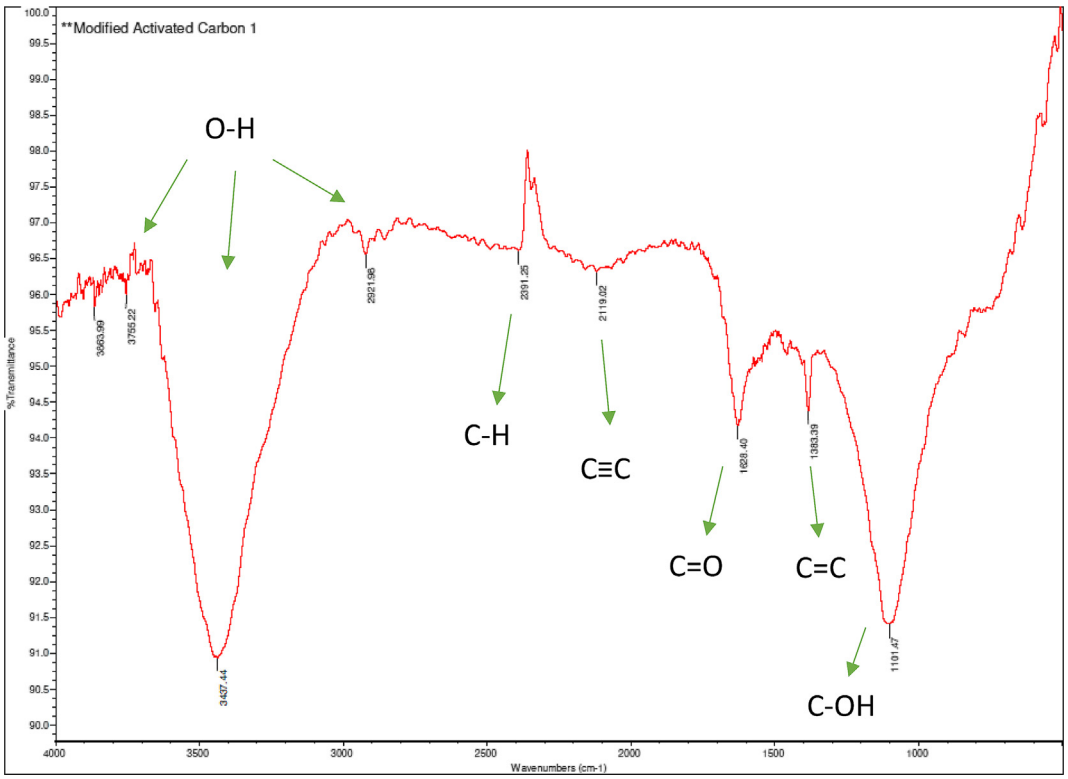

Figure 6. FT-IR spectra of AC/MWCNT.

percentages of zinc and chlorine came from the activation agent, the low level of nitrogen came from the uniformly flowing nitrogen gas during the carbonization process and oxygen came from the organic material itself [33]. Figure 4b shows the elements present after the sample has been washed with 1.0M HCl and deionized water. It can be observed from the figure that the amounts of zinc and chlorine were greatly reduced which implies that the washing eliminated most of the zinc and chlorine residues resulting to the formation of pores in the sample.

X-ray diffraction was used for the identification of the crystalline structure of the samples. The diffraction peaks of the AC/MWCNT sample are shown in Figure 5. The noticeable hump in the 2 theta range, 20°–30°, signifies a high degree of disorder which is very common in carbonaceous materials. The (002) peak corresponding to a d-spacing between graphene sheets of 3.42–3.46 Å and the (100) peak at 43° are attributed to the in-plane graphitic structure of the multiwalled carbon nanotubes. The peaks at 38.2° and 44.5° signifying the presence of ZnO in the activated carbon verifies the EDX results.

The chemical composition of the AC/MWCNT sample was studied using Fourier-transform infrared spectroscopy. The FT-IR spectra of the sample is shown in Figure 6. The dip at approximately 1100 cm^{-1} corresponds to the C–OH stretch vibration while the dip at approximately 1400 cm^{-1} is attributed to C=C symmetrical stretching. A C=O stretching vibration of the carboxylic acid was identified at the 1650 cm^{-1} dip. The dip at approximately 2300 cm^{-1} corresponds to a C≡C stretch which signifies the MWCNT bonds. The dip at approximately 2350 cm^{-1} indicates a C–H stretch and the dip at approximately 3400 cm^{-1} is characteristic of the hydroxyl group showing an O–H stretch.

3.3. Cyclic voltammetry

Cyclic voltammetry was performed to study the performance of the AC/MWCNT electrodes. The specific capacitance C was calculated from the resulting cyclic voltammograms using [34].

$$C = \frac{\int I\, dv}{vm\Delta V} \quad (1)$$

where the integrated area under the CV curve I is the oxidation or reduction current (A), v is the scan rate (V/s), m is the mass of the electrode material (g), and ΔV is the voltage range (V).

3.3.1. Three-electrode system

The CV curves of the electrodes are shown in Figure 7. It can be observed from the figure that the CV curve of the electrode fabricated using sample A shows a large peak at the bottom suggesting that oxidation took place. The electrodes fabricated using samples B, G and H also show oxidation peaks but much smaller than that of sample A. The electrode fabricated using sample C shows two peaks at either side of the curve which suggests that both reduction and oxidation took place. Figures 7d-7f show that reduction and oxidation did not take place in samples D, E, and F. According to Eq. (1), capacitance is directly proportional to the area of the curves generated by the cyclic voltammetry scan. It can be seen from the CV curves that the samples with a MOFS to $ZnCl_2$ weight ratio of 1:3 have smaller areas enclosed by the CV curves as compared to their 1:2 counterparts. Hence, their capacitance, energy density, and power density are lower than those of their 1:2 counterparts (Table 2). The redox reaction that took place in the CV scans and the lower capacitance output of the 1:3 samples are due to the greater amounts of $ZnCl_2$ residues that were not washed away by HCl and hence less pores were formed [35]. It can be seen in Table 2 that the electrode with a MOFS to $ZnCl_2$ weight ratio of 1:2 at 800 °C carbonization temperature was observed to have the highest specific capacitance, average energy density, and average power density, hence, it was used for the remaining tests. It can also be observed from the table that the addition of MWCNT to AC enhanced the capacity of the elecrode.

3.3.2. Two-electrode system

The CV curves of the EDLC are shown in Figure 8. It can be seen in the figure that the CV curves maintained their shape at different scan rates

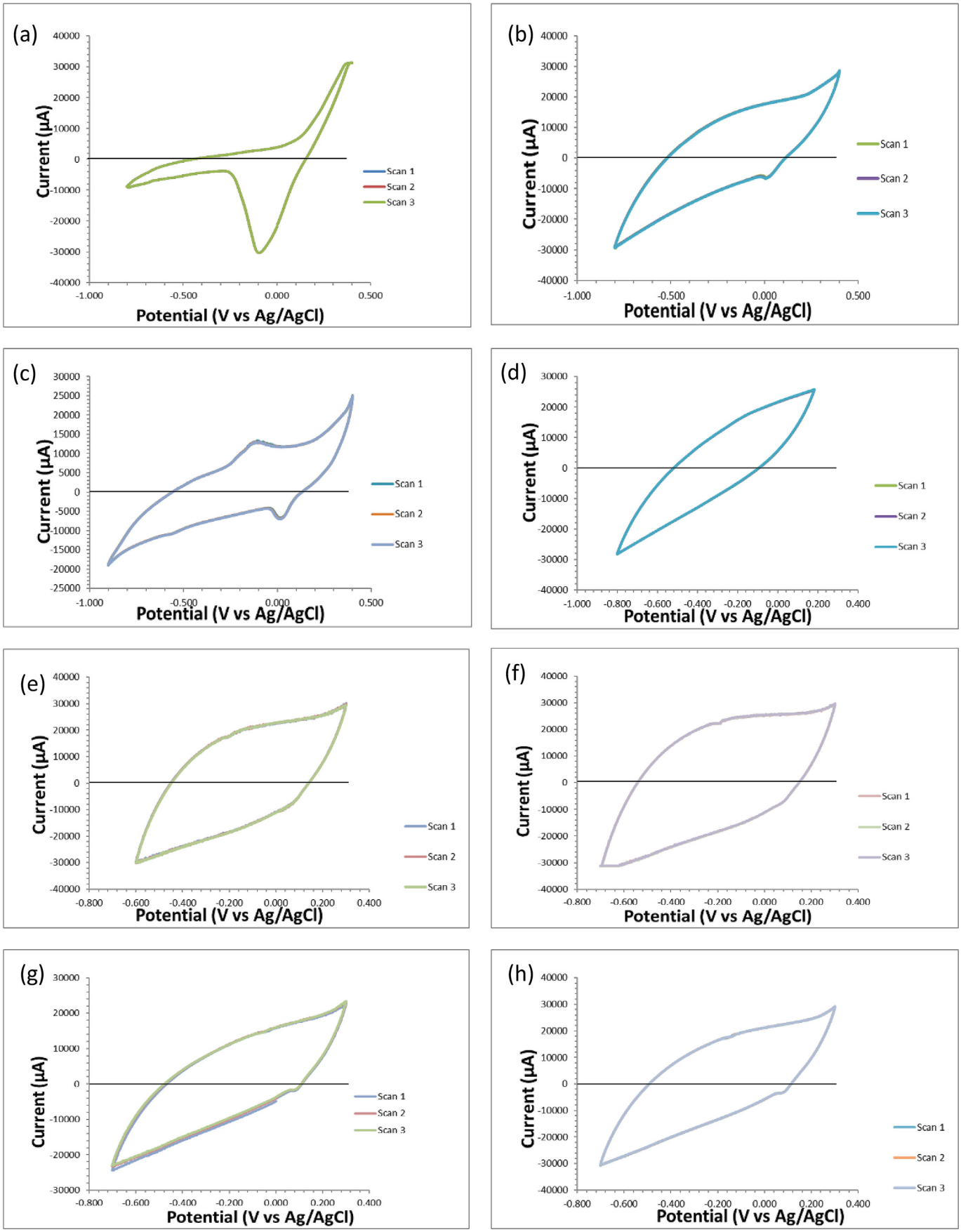

Figure 7. CV curves of the electrodes fabricated using activated carbon (a) sample A, (b) sample B, (c) sample C, (d) sample D, (e) sample E, (f) sample F, (g) sample G, and (h) sample H.

Table 2. Values obtained in terms of capacitance, average energy density, and average power density of each sample.

Sample	A	B	C	D	E	F	G	(F w/o MWCNT)	EDLC
Capacitance (F g^{-1})	47	122	78	116	124	130	94	126	122
Avg. energy density (W h kg^{-1})	7	17	11	16	17	18	13	18	17
Avg. power density (kW kg^{-1})	0.6	1.5	1.0	1.4	1.5	1.6	1.1	1.6	1.5

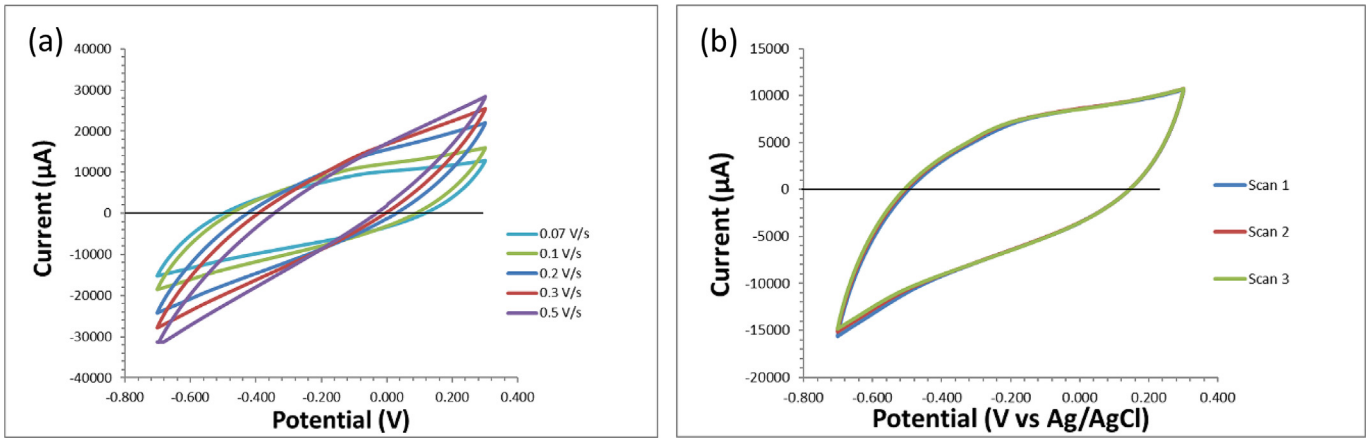

Figure 8. CV curves of the EDLC (a) at different scan rates and (b) for three scans.

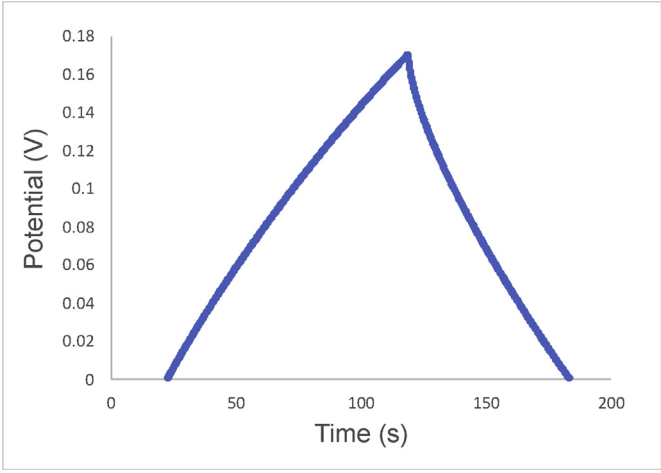

Figure 9. Galvanostatic charge-discharge curve of the EDLC.

and multiple scans indicating that the EDLC has excellent capacitive characteristics and reversibility [34]. The two electrode system yields values approximately half of the capacitance of the three-electrode system while the mass of the electrode doubles [36]. In this case, calculating for the specific capacitance of the two electrode system requires a multiplier of 4 in Eq. (1) to adjust the capacitance of the cell and the combined mass of the two electrodes to the capacitance and mass of a single electrode. A two-electrode system generates almost half the capacitance value compared to a three-electrode system hence the resulting capacitance should be doubled and since a two-electrode system uses two symmetrical working electrodes, another multiplier of 2 is needed to adjust the value to its specific capacitance. The specific capacitance of the fabricated EDLC was found to be 122 F g^{-1} at a current density of 0.5 A g^{-1} and the average energy density and average power density are 17 W h kg^{-1}, and 1.5 kW kg^{-1}, respectively (Table 2).

3.4. Chronopotentiometry

The two-electrode system was used for chronopotentiometry over a potential range of -0.1 V–0.2 V and current density of 0.5 A g^{-1}. The

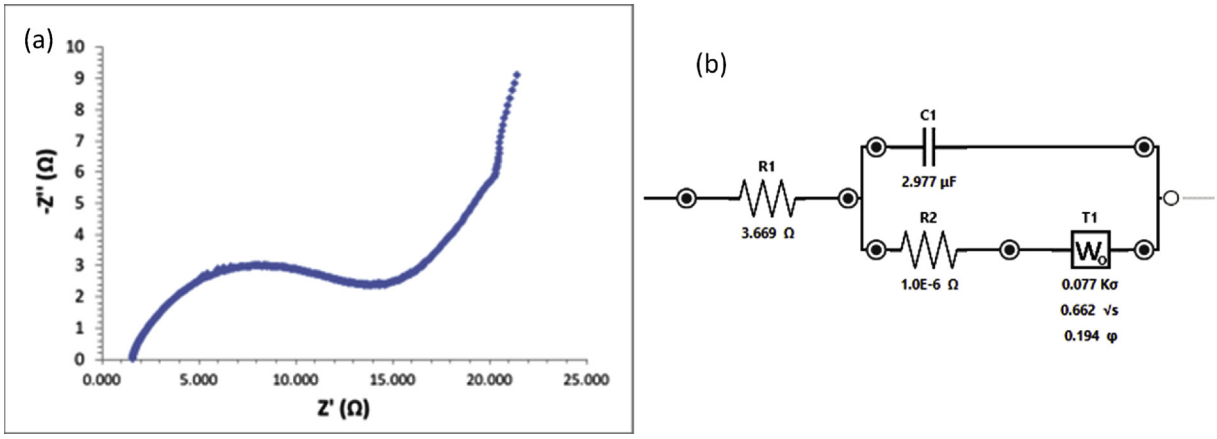

Figure 10. (a) Nyquist plot of the fabricated EDLC, and (b) the equivalent circuit used for fitting of EIS measurements.

Table 3. Performance comparison of the fabricated EDLC with previous works.

Electrode Material	Electrolyte	Current Density (A g^{-1})	Potential range (V)	Specific capacitance (F g^{-1})	Ref.
CNT/Microporous carbon	3 M H_2SO_4	0.1–50	0.9	125–237	[42]
Graphene-coated CNT aerogel	EMI-TFSI*	0.01–10	3.0	60–130	[43]
Graphene/CNT composite fibers	0.5 M H_2SO_4	0.2–2	0.8	6–35	[44]
Carbonized PPy** nanotubes	1 M KCl		1.5	40–140	[45]
Carbonized halogen-containing plastic waste	6 M KOH	0.5–40	1.0	110–313	[46]
Activated carbon/CNT	-	5	0.8	96–213	[28]
Activated MOFS carbon/MWCNT	3M KOH	0.5	1.2	122	This work

* 1-ethyl-3-methylimidazolium bis(trifluoromethylsulfonyl)imide.
** Polypyrrole.

triangular-shaped GCD profile (Figure 9) shows good symmetry and nearly linear discharge slope, implying that the EDLC has excellent reversibility and capacitive characteristics [37, 38] confirming the CV result. A small potential drop (<0.013 V) was observed suggesting that the fabricated EDLC has a low internal resistance [39].

3.5. Electrochemical impedance spectroscopy

Using the two-electrode system, an EIS scan was run over the frequency range of 1 MHz–100 Hz. The resulting Nyquist plot (Figure 10a) is comparable to the usual shape of Nyquist plots of most EDLCs, wherein a semi-circle occurs at higher frequencies, followed by a nonvertical line at intermediate frequencies and a nearly vertical line at lower frequencies [40]. The semi-circle in the plot is related to the EDLC's resistance, the nonvertical line is related to the ion transport limitation in the electrolyte and the nearly vertical line is related to the dominant capacitive behavior of the electric double layer formed at the electrode/electrolyte interface [40, 41]. The low equivalent series resistance or internal resistance of the EDLC (1.6 Ω) which was obtained from the x-intercept of the semi-circle in the plot confirms the GCD result. The nearly vertical line in the low frequency region suggests that the EDLC has an excellent capacitive behavior [31] confirming the CV and GCD results. An equivalent circuit (Figure 10 b) was generated by fitting the EIS data. The Randles circuit shows an electrolyte resistance (R1) value of 3.7 Ω, a charge transfer resistance (R2) value of 1.0 μΩ, a double layer capacitance (C1) value of 3.0 μF, and the Warburg open (W_O) elements with values of 0.077 for Kσ, 0.66 for $\sqrt{s}$, and 0.19 for φ.

3.6. Comparison with other works

Table 3 shows the performance comparison of the fabricated EDLC with previous works. It can be seen from the table that the performance of the fabricated EDLC in terms of specific capacitance is at par with those in the literature. Further improvements in the fabrication of the MOFS/MWCNT electrodes is recommended to further increase the specific capacitance of the EDLC.

4. Conclusions

The fabrication and characterization of an electric double-layer supercapacitor based on multi-walled carbon nanotube and activated carbon synthesized from *Moringa Oleifera* fruit shell was reported. Scanning electron microscopy and EDX results revealed that activation of the carbonized fruit shells by $ZnCl_2$ and subsequent washing by HCl resulted in the removal of zinc and chlorine residues which lead to the formation of pores. The activated carbon with a 1:2 MOFS to $ZnCl_2$ weight ratio and carbonization temperature of 800 °C obtained the highest capacitance of 130 F g^{-1}, hence, it was used to fabricate the electrodes of the EDLC. Electrochemical characterization using CV, chronopotentiometry and EIS revealed that the fabricated EDLC has excellent capacitive characteristics and low internal resistance. The specific capacitance of the EDLC was found to be 122 F g^{-1} at a current density of 0.5 A g^{-1}, average energy density of 17 W h kg^{-1}, average power density of 1.5 kW kg^{-1} and an equivalent resistance of 1.6 Ω. After 100 scans with a scan rate of 0.1 V s^{-1}, the percent decrease in capacitance was calculated to be 2.65% of its original capacitance.

Declarations

Author contribution statement

Shirley Palisoc & Michelle Natividad: Conceived and designed the experiments; Performed the experiments; Contributed reagents, materials, analysis tools or data; Wrote the paper.

Joshua Marco Dungo: Performed the experiments; Analyzed and interpreted the data; Wrote the paper.

Funding statement

This research did not receive any specific grant from funding agencies in the public, commercial, or not-for-profit sectors.

Competing interest statement

The authors declare no conflict of interest.

Additional information

No additional information is available for this paper.

References

[1] A. González, E. Goikolea, J.A. Barrena, R. Mysyk, Review on supercapacitors: technologies and materials, Renew. Sustain. Energy Rev. 58 (2016) 1189–1206.
[2] P. Simon, Y. Gogotsi, B. Dunn, Where do batteries end and supercapacitors begin? Science 343 (6176) (2014) 1210–1211.
[3] F. Béguin, E. Frąckowiak, Supercapacitors: Materials, Systems, and Applications, Wiley-VCH, Weinheim, 2013.
[4] S. Najib, E. Erdem, Current progress achieved in novel materials for supercapacitor electrodes: mini review, Nanoscale Advances 1 (2019) 2817–2827.
[5] M. Gidwani, A. Bhagwani, N. Rohra, Supercapacitors: the near future of batteries, Int. J. Od Eng. Invent. 4 (5) (2014) 22–27.
[6] D. Qu, H. Shi, Studies of activated carbons used in double-layer capacitors, J. Power Sources 74 (1) (1998) 99–107.
[7] M. Palada, The moringa industry in the Philippines: status, challenges and opportunities, Acta Hortic. (Wagening.) (1158) (2017) 447–454.
[8] B. Lou, P. Veerakumar, S. Chen, V. Veeramani, R. Madhu, S. Liu, Ruthenium nanoparticles decorated curl-like porous carbons for high performance supercapacitors, Sci. Rep. 6 (1) (2016).
[9] Z. Tehrani, D. Thomas, T. Korochkina, C. Phillips, D. Lupo, S. Lehtimäki, J. O'Mahony, D. Gethin, Large-area printed supercapacitor technology for low-cost domestic green energy storage, Energy 118 (2017) 1313–1321.
[10] Y. Zhu, S. Murali, M.D. Stoller, K.J. Ganesh, P.J. Ferreira, A. Pirkle, R.M. Wallace, K.A. Cychosz, M. Thommes, D. Su, E.A. Stach, R.S. Ruoff, Carbon-based supercapacitors produced by activation of graphene, Science 332 (2011) 1537–1541.

[11] M. Deraman, N. Nor, N. Basri, B. Dollah, S. Soltaninejad, R. Daik, R. Omar, M.A. Hashim, M.A.R. Othman, Graphene and activated carbon based supercapacitor electrodes, Adv. Mater. Res. 1112 (2015) 231–235.
[12] J.M. Lee, T. Wu, B.M. Alston, M.E. Briggs, T. Hasell, C. Hu, A.I. Cooper, Porosity-engineered carbons for supercapacitive energy storage using conjugated microporous polymer precursors, J. Mater. Chem. 4 (2016) 7665–7673.
[13] D. Wang, Z. Geng, B. Li, C. Zhang, High performance electrode materials for electric double double-layer capacitors based on biomass-derived activated carbons, Electrochim. Acta 173 (2015) 377–384.
[14] M. Wu, P. Li, Y. Li, J. Liu, Y. Wang, Enteromorpha based porous carbons activated by zinc chloride for supercapacitors with high capacity retention, RSC Adv. 5 (2015) 16575–16581.
[15] H. Wang, Z. Xu, A. Kohandehghan, K. Cui, X. Tan, T.J. Stephenson, C.K. King'ondu, C.M. Holt, B.C. Olsen, J.K. Tak, D. Harfield, A.O. Anyia, D. Mitlin, Interconnected carbon nanosheets derived from hemp for ultrafast supercapacitors with high energy, ACS Nano 7 (2013) 5131–5141.
[16] L. Kouchachvili, N. Maffei, E. Entchev, Infested ash trees as a carbon source for supercapacitor electrodes, J. Porous Mater. 22 (2015) 979–988.
[17] Y. Luan, L. Wang, S. Guo, B. Jiang, D. Zhao, H. Yan, C. Tiana, H. Fu, A hierarchical porous carbon material from a loofah sponge network for high performance supercapacitors, RSC Adv. 5 (2015) 42430–42437.
[18] Y. Li, Y.A. Samad, K. Polychronopoulou, S. Alhassan, K. Liao, From biomass to high performance solar solar-thermal and electric electric-thermal energy conversion and storage materials, J. Mater. Chem. 2 (2014) 7759–7765.
[19] E. Redondo, J. Carretero Carretero-González, E. Goikolea, J. Ségalini, R. Mysyk, Effect of pore texture on performance of activated carbon supercapacitor electrodes derived from olive pits, Electrochim. Acta 160 (2015) 178178–178184.
[20] K. Karthikeyan, S. Amaresh, S.N. Lee, X. Sun, V. Aravindan, Y. Lee, Y.S. Lee, Construction of high-energy-density supercapacitors from pine-cone–derived high-surface-area carbons, ChemsSusChem 7 (2014) 1435–1442.
[21] M. Wu, R. Li, X. He, H. Zhang, W. Sui, M. Tan, Microwave-assisted preparation of peanut shell shell-based activated carbons and their use in electrochemical capacitors, N. Carbon Mater. 30 (2015) 86–91.
[22] M. Wu, L. Li, J. Liu, Y. Li, P. Ai, W. Wu, J. Zheng, Template-free preparation of mesoporous carbon from rice husks for use in supercapacitors, N. Carbon Mater. 30 (2015) 471–475.
[23] M. Wu, P. Ai, M. Tan, B. Jiang, Y. Li, J. Zheng, W. Wu, Z. Li, Q. Zhang, X. He, Synthesis of starch starch-derived mesoporous carbon for electric double layer capacitor, Chem. Eng. J. 245 (2014) 166–172.
[24] P. Cheng, S. Gao, P. Zang, X. Yang, Y. Bai, H. Xu, Z. Liu, Z. Lei, Hierarchically porous carbon by activation of shiitake mushroom for capacitive energy storage, Carbon 93 (2015) 315–324.
[25] H. Chen, Y. Guo, F. Wang, G. Wang, P. Qi, X. Guo, B. Dai, F. Yu, An activated carbon derived from tobacco waste for use as a supercapacitor electrode material, N. Carbon Mater. 32 (6) (2017) 592–599.
[26] K. Wang, N. Zhao, S. Lei, R. Yan, X. Tian, J. Wang, Y. Song, D. Xu, Q. Guo, L. Liu, Promising biomass-based activated carbons derived from willow catkins for high performance supercapacitors, Electrochim. Acta 166 (2015) 1–11.
[27] F. Markoulidis, C. Lei, C. Lekakou, D. Duff, S. Khalil, B. Martorana, I. Cannavaro, A method to increase the energy density of supercapacitor cells by the addition of multiwall carbon nanotubes into activated carbon electrodes, Carbon 68 (2014) 58–66.
[28] O. Ibukun, H.K. Jeong, An activated carbon and carbon nanotube composite for a high-performance capacitor, New Physics: Sae Mulli 68 (2) (2018) 185–188.
[29] O.S. Bello, K.A. Adegoke, O.O. Akinyunni, Preparation and characterization of a novel adsorbent rom Moringa oleifera leaf, Appl. Water Sci. 7 (2017) 1295–1305.
[30] N.K. Amaglo, et al., Profiling selected phytochemicals and nutrients in different tissues of multipurpose tree Moringa oleifera L., grown in Ghana, Food Chem. 122 (2010) 1047–1054.
[31] C. Contescu, S. Adhikari, N. Gallego, N. Evans, B. Biss, Activated carbons derived from high-temperature pyrolysis of lignocellulosic biomass, J. Carbon Res. 4 (2018) 1–16.
[32] Z. Li, Z. Zhou, G. Yun, K. Shi, X. Lv, B. Yang, High-performance solid-state supercapacitors based on graphene-ZnO hybrid nanocomposites, Nanoscale Res. Lett. 8 (1) (2013).
[33] K. Scott, Electrochemical principles and characterization of bioelectrochemical systems, Microb. Electrochem. Fuel Cells (2016) 29–66.
[34] P. Wang, T. Wang, W. Lin, H. Lin, M. Lee, C. Yang, Enhanced supercapacitor performance using electropolymerization of self-doped polyaniline on carbon film, Nanomaterials 8 (2018) 1–12.
[35] E. Frackowiak, F. Béguin, Carbon materials for the electrochemical storage of energy in capacitors, Carbon 39 (6) (2001) 937–950.
[36] Y.J. Kang, H. Chung, C. Han, W. Kim, All-solid-state flexible supercapacitors based on papers coated with carbon nanotubes and ionic-liquid-based gel electrolytes, Nanotechnology 23 (28) (2012) 289501.
[37] M. Fahim, A. Shah, S. Bila, Highly stable and efficient performance of binder-free symmetric supercapacitor fabricated with electroactive polymer synthesized via interfacial polymerization, Materials 12 (2019) 1–17.
[38] Y. Zhou, P. Jin, Y. Zhou, Y. Zhu, High-performance symmetric supercapacitors based on carbon nanotube/graphite nanofiber nanocomposites, Sci. Rep. 8 (2017) 1–7.
[39] J. Wu, F. Ge, Y. Li, Preparation of Ni(OH)2/MWCNTs composite for supercapacitor application, Int. J. Electrochem. Sci. 12 (2017) 9665–9674.
[40] B. Mei, O. Munteshari, J. Lau, B. Dunn, L. Pilon, Physical interpretations of nyquist plots for EDLC electrodes and devices, J. Phys. Chem. 122 (2018) 194–206.
[41] H. Yang, S. Kannappan, A. Pandian, J. Jang, Y. Lee, W. Lu, Graphene supercapacitor with both highpower and energy density, Nanotechnology 28 (2017) 1–10.
[42] Y. Yao, C. Ma, J. Wang, W. Qiao, L. Ling, D. Long, Rational design of high-surface-area carbon nanotube/microporous carbon core–shell nanocomposites for supercapacitor electrodes, ACS Appl. Mater. Interfaces 7 (2015) 4817–4825.
[43] E. Wilson, M.F. Islam, Ultracompressible, high-rate supercapacitors from graphene-coated carbon nanotube aerogels, ACS Appl. Mater. Interfaces 7 (2015) 5612–5618.
[44] H. Sun, X. You, J. Deng, X. Chen, Z. Yang, J. Ren, H. Peng, Novel graphene/carbon nanotube composite fibers for efficient wire-shaped miniature energy devices, Adv. Mater. 26 (2014) 2868–2873.
[45] C. Ćirić-Marjanović, S. Mentus, I. Pašti, N. Gavrilov, J. Krstić, J. Travas-Sejdic, L.T. Strover, J. Kopecká, Z. Moravková, M. Trchová, J. Stejskal, Synthesis, characterization, and electrochemistry of nanotubular polypyrrole and polypyrrole-derived carbon nanotubes, J. Phys. Chem. C 118 (2014) 14770–14784.
[46] X.Y. Chen, L.X. Cheng, X. Deng, L. Zhang, Z.J. Zhang, Generalized conversion of halogen-containing plastic waste into nanoporous carbon by a template carbonization method, Ind. Eng. Chem. Res. 53 (2014) 6990–6997.